Appl Phys B (2010) 100: 891–896
DOI 10.1007/s00340-010-4128-1

Applied Physics B
Lasers and Optics

Effect of etching parameters on antireflection properties of Si subwavelength grating structures for solar cell applications

J.W. Leem · Y.M. Song · Y.T. Lee · J.S. Yu

Received: 1 December 2009 / Revised version: 5 May 2010 / Published online: 10 July 2010

Abstract Silicon (Si) subwavelength grating (SWG) structures were fabricated on Si substrates by holographic lithography and subsequent inductively coupled plasma (ICP) etching process using $SiCl_4$ with or without Ar addition for solar cell applications. To ensure a good nanosized pattern transfer into the underlying Si layer, the etch selectivity of Si over the photoresist mask is optimized by varying the etching parameters, thus improving antireflection characteristics. For antireflection analysis of Si SWG surfaces, the optical reflectivity is measured experimentally and it is also calculated theoretically by a rigorous coupled-wave analysis. The reflectance depends on the height, period, and shape of two-dimensional periodic Si subwavelength structures, correlated with ICP etching parameters. The optimized Si SWG structure exhibits a dramatic decrease in optical reflection of the Si surface over a wide angle of incident light (θ_i), i.e. less than 5% at wavelengths of 300–1100 nm, leading to good wide-angle antireflection characteristics (i.e. solar-weighted reflection of 1.7–4.9% at $\theta_i < 50°$) of Si solar cells.

J.W. Leem · J.S. Yu (✉)
Department of Electronics and Radio Engineering, Kyung Hee University, 1 Seocheon-dong, Giheung-gu, Yongin-si, Gyeonggi-do 446-701, Republic of Korea
e-mail: jsyu@khu.ac.kr

Y.M. Song · Y.T. Lee
Department of Information and Communications, Gwangju Institute of Science and Technology, 1 Oryong-dong, Buk-gu, Gwangju 500-712, Republic of Korea

Y.T. Lee
e-mail: ytlee@gist.ac.kr

1 Introduction

There has been a growing interest in low-cost broadband antireflection coatings (ARCs) for various device applications. Optoelectronic devices including solar cells, photodetectors, and displays require antireflection layers to suppress the surface reflection of an optical window over a wide wavelength range [1–3]. Recently, periodic nanostructures with a period smaller than the incident light wavelength which can lead to an effective refractive-index gradient between the semiconductor and the air have attracted much attention for antireflection properties, showing long-term thermal stability as well as good durability [4, 5]. Thus, subwavelength grating (SWG) structures with optimized shapes have appeared as a more promising candidate for ARC applications compared to the conventional single-layer or multilayer thin films [6–8]. Electron-beam lithography or nanoimprint lithography is widely used to fabricate nanosized patterns, but it is expensive and complex [9, 10]. Holographic lithography is a simple, fast, cost-effective, and large-scale technique, allowing for an economical production process [11, 12].

Especially, for thin-film Si solar cells, efficient light incoupling is crucial because of their low optical absorption coefficient. In order to improve the efficiency in Si-based solar cells, it is necessary to employ broadband and omnidirectional ARCs which can cover a wavelength range of the solar spectrum. However, it is inherently difficult for single-layer ARCs to cover a broad wavelength range. Although multilayer ARCs can overcome this problem, they require more expensive fabrication and critical layer thickness control [13]. The SWG structures can be used for the fabrication of wide-angle broadband antireflection surfaces in solar cells. Antireflection characteristics depend strongly on the size, shape, and array geometry of the SWGs. The etch selectivity can affect the aspect ratio of the SWG structures. For solar cell applications, it is essential to reduce the

solar-weighted reflection (SWR) over a wide angle of incident light. In this paper, we fabricated optimally antireflective Si SWGs by properly controlling the process conditions using both holographic lithography and inductively coupled plasma (ICP) etching for solar cell applications. The optical reflectivity of fabricated SWG structures was measured and compared to that from numerical simulation based on rigorous coupled-wave analysis (RCWA). The influence of the angle of incidence on the reflectance and SWR was also investigated for the optimized Si SWG structures.

2 Experimental details

Figure 1a shows the schematic diagram of the pattern transfer process steps for the fabrication of the Si SWG structures on Si substrates. For the fabrication of Si SWG structures, AZ5206 photoresist (PR) was deposited on Si substrates by a spin coating process. The PR thickness decreased with the increase of dilution and rotation speed. The dilution and rotation speed were determined to obtain the desired optimum PR thickness. After prebaking on a hot plate at 90°C for 90 s, the PR was then exposed twice by the interference of two crossed beams using an Ar-ion laser operating at a wavelength of 363.8 nm to form two-dimensional periodic nanosized PR patterns. The grating period (Λ) of the PR patterns is given by the well-known equation $\Lambda = \lambda/[2\sin(\theta/2)]$, where λ is the laser source wavelength and θ is the angle between the two beams [14]. Thus, the grating period can be easily controlled by varying θ, which is adjusted by rotating the rotation stage. For a hexagonal pattern, the sample was rotated by 60° between exposures. After the development, the nanosized patterns are transferred from the PR into the Si surface by using ICP etching for SWG structures. For high etch selectivity of Si to the nanosized PR pattern, it was found that $SiCl_4$ is superior to SF_6 in ICP etching. The underlying Si was etched in $SiCl_4$ plasma with or without Ar addition at room temperature. The overall etching of the PR-patterned Si substrate until complete removal of PR leads to extremely fast etching at the rim and slower etching at the center, producing a smooth tapered profile grating. For a desirable etched profile, the etch rate and etch selectivity can be controlled by varying etching parameters including RF power, $SiCl_4$ flow rate, and additional Ar flow rate. The RF power was changed from 25 W to 100 W and the $SiCl_4$ flow rate was changed from 2.5 sccm to 10 sccm. Ar of 0–20 sccm was added in the $SiCl_4$ plasma. The process pressure was fixed at 10 mTorr. From scanning electron microscope (SEM) measurements, the etched profile and depth of fabricated Si SWG structures were observed. The optical reflectivity was measured by using a UV–Vis–NIR spectrophotometer and spectroscopic ellipsometer.

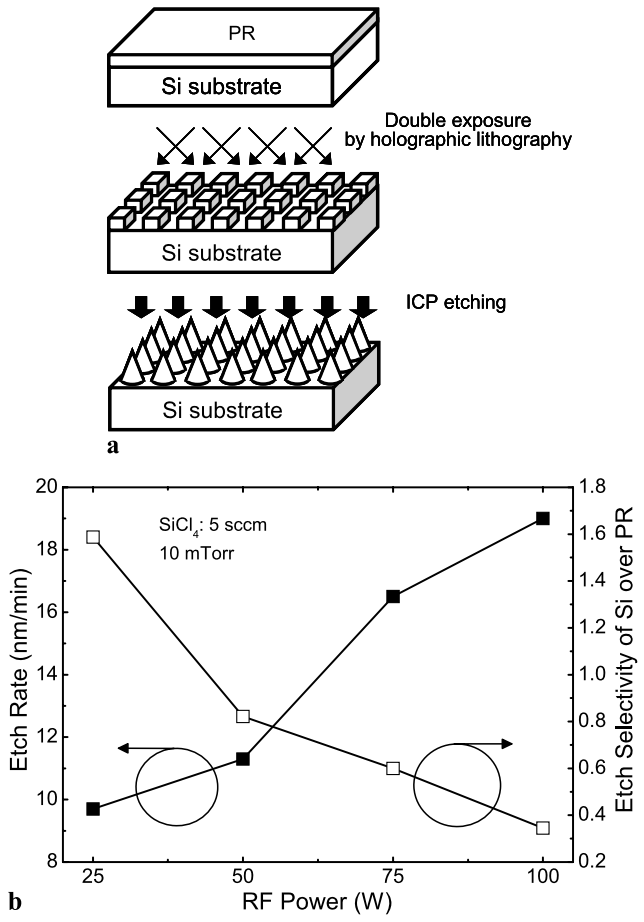

Fig. 1 (**a**) Schematic diagram of the pattern transfer process steps for the fabrication of the Si SWG structures on Si substrates and (**b**) etch rate of Si and etch selectivity of Si over PR as a function of RF power

3 Results and discussion

The etched profile, which is closely associated with the optical reflectivity of the Si surface, depends strongly on the etch selectivity of Si over PR during the overall etching. To obtain good antireflection characteristics, therefore, the etching parameters should be optimized with a desirable etched profile in terms of etch rate and etch selectivity. Figure 1b shows the etch rate of Si and etch selectivity of Si over PR as a function of RF power. The $SiCl_4$ flow rate was 5 sccm and the process pressure was 10 mTorr. The density of active particles in the ion energy flux increases with RF power. Thus, the etch rate of Si increased from 9.7 nm/min at 25 W to 19 nm/min at 100 W as the RF power was increased. The RF power also has a strong effect on the etch selectivity of Si over PR. The etch selectivity was decreased from 1.6 at 25 W to 0.3 at 100 W with increasing the RF power due to the enhanced erosion of the PR mask pattern.

Figure 2a shows the SEM images of the etched Si SWG structures with a pattern period of 300 nm for different RF

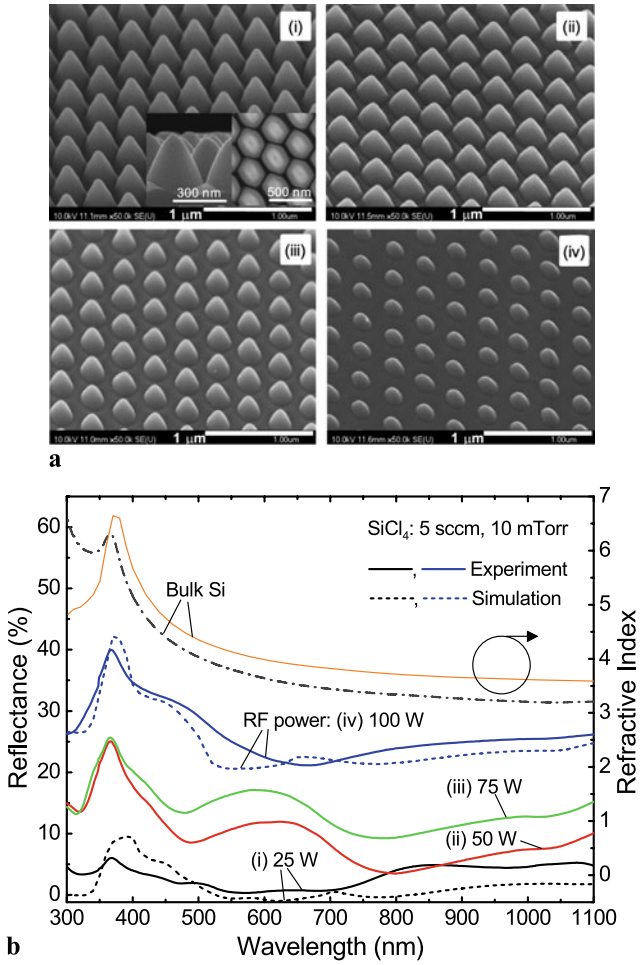

Fig. 2 (**a**) SEM images and (**b**) measured reflectance spectra of the etched Si SWG structures with a pattern period of 300 nm for different RF powers: (i) 25 W, (ii) 50 W, (iii) 75 W, and (iv) 100 W. The top- and side-view SEM images of the etched structures are shown in (i) of (**a**). For comparison, the calculated reflectance spectra for the Si SWG structures etched at 25 W and 100 W are shown in (**b**). The refractive index of bulk Si used in this calculation is also shown

powers: (i) 25 W, (ii) 50 W, (iii) 75 W, and (iv) 100 W. The top-view SEM image of the etched structures exhibits two-dimensional periodic hexagonal nanopatterns as shown in the inset of (i) of Fig. 2a. The etched depth was decreased with increasing the RF power due to the reduced etch selectivity of Si over PR. At 100 W, it is noted that the depth was very low with an etched dot array. At 25 W, the etched structure exhibited a gradually tapered conical shape (side view) in a closely packed arrangement due to the high etch rate and etch selectivity as shown in the inset of (i) of Fig. 2a. Figure 2b shows the measured reflectance as a function of wavelength for the etched Si SWG structures with a pattern period of 300 nm at (i) 25 W, (ii) 50 W, (iii) 75 W, and (iv) 100 W. For comparison, the calculated reflectance spectra for the Si SWG structures etched at 25 W and 100 W are shown in Fig. 2b. The refractive index of bulk Si used in this calculation is also shown. The specular reflectance was measured by linearly polarized light at normal incidence. The reflectance of the bulk Si substrate is also shown as a reference. For bulk Si, the reflectance was high, i.e. more than 32% over a wavelength of 300–1100 nm. The reflectance was reduced in a wide wavelength range as the RF power was decreased. As expected, the reflectance depends strongly on the etched profile of the array patterns. At 100 W, the reflectance was reduced compared to the bulk Si despite the dot array pattern with low heights as shown in (iv) of Fig. 2a. The calculated and measured results give a reasonable consistency, though there exist slight differences in some wavelength regions. For the smooth tapered conical structure fabricated at 25 W, the reflectance was significantly reduced to less than 5% in the visible and near-infrared wavelength regions and it was lower than 0.75% at the wavelengths of 535–700 nm.

Figure 3 shows the measured reflectance spectra of the etched Si SWG structures with a pattern period of 300 nm (a) for different $SiCl_4$ flow rates and (b) for different flow rates of additional Ar. The reflectance was lowest on average (especially, $\lambda < 630$ nm) at 5 sccm of $SiCl_4$, and it was increased with the increase or decrease of $SiCl_4$ flow rate. Around $\lambda \sim 370$ nm, there is a strong variation of reflectance because Si has a relatively high refractive index at this wavelength. The etch rate and etch selectivity of Si over PR as a function of $SiCl_4$ flow rate at 25 W and 10 mTorr are shown in the right-hand inset of Fig. 3a. Although there is no considerable change in the etch rate for $SiCl_4$ flow rates of 2.5–10 sccm, the highest etch rate and etch selectivity were observed at 5 sccm of $SiCl_4$. The increase in chemical reactant species of $SiCl_4$ enhances chemical etching with a reduced etch selectivity, leading to a smoothly rounded conical shape as shown in the left-hand inset of Fig. 3a. At 2.5 sccm of $SiCl_4$, the increased reflectance may be ascribed to the low etch rate and etch selectivity by low chemical reactant species. As shown in Fig. 3b, the reflectance was increased on average (especially, $\lambda < 750$ nm) as the additional Ar flow rate to $SiCl_4$ was increased. The right-hand inset of Fig. 3b shows the etch rate and etch selectivity of Si over PR as a function of Ar flow rate in 5 sccm of $SiCl_4$ at 25 W and 10 mTorr. With addition of 20 sccm Ar, the etch rate was decreased to 5 nm/min and the etch selectivity was also reduced to 0.7. This means that the 5 sccm of $SiCl_4$ is enough to obtain the highest etch rate as seen in the right-hand inset of Fig. 3a. The Ar addition prevents the chemical reactant species. The reduction in etch selectivity is probably due to the increased PR erosion rate.

Figure 4a shows the measured reflectance of the etched Si SWG structures in 5 sccm of $SiCl_4$ plasma at 25 W and 10 mTorr as a function of wavelength for the periods of 300 nm, 400 nm, and 500 nm. The SEM images of the Si SWG structures with different periods are shown in the inset of Fig. 4a. The period of the PR patterns was changed by tuning the rotation stage angle and the patterns were transferred to the Si

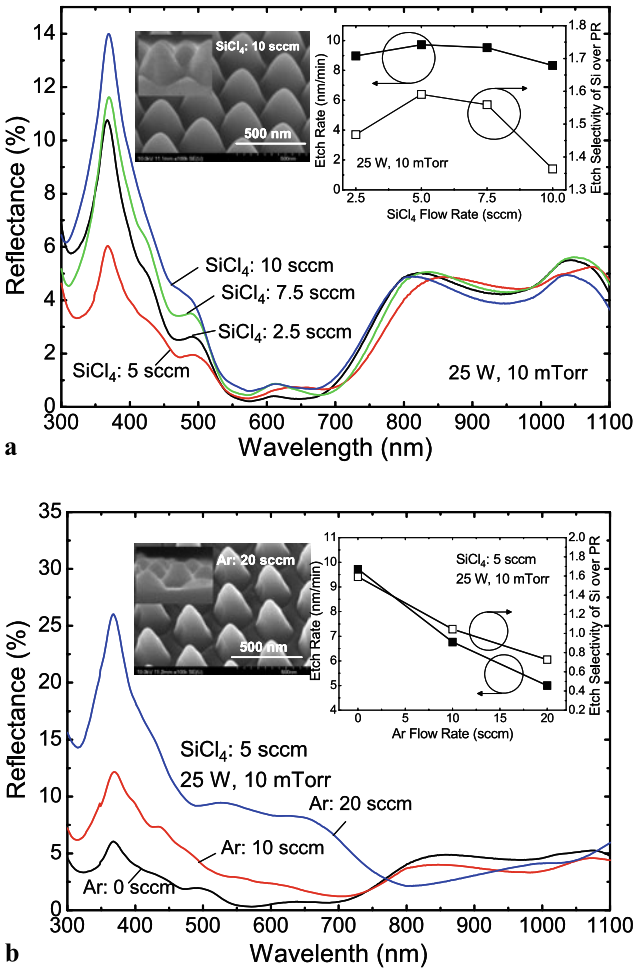

Fig. 3 Measured reflectance spectra of the etched Si SWG structures with a pattern period of 300 nm (**a**) for different $SiCl_4$ flow rates and (**b**) for different flow rates of additional Ar. The left-hand insets of (**a**) and (**b**) show the SEM images of Si SWGs for $SiCl_4$ of 10 sccm and for Ar of 20 sccm, respectively. The right-hand insets of (**a**) and (**b**) show the etch rate and etch selectivity as functions of $SiCl_4$ flow rate and Ar flow rate, respectively

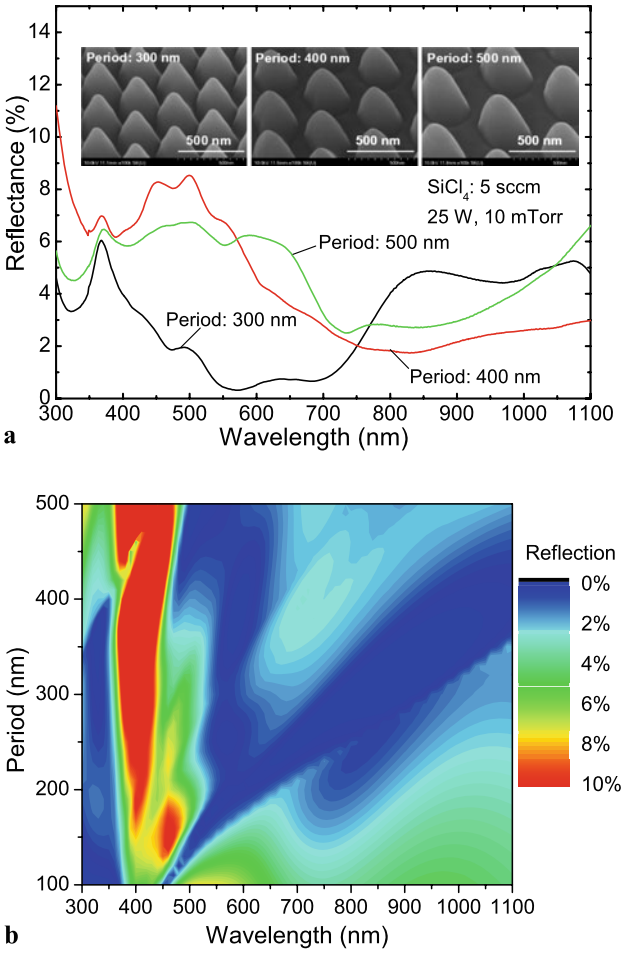

Fig. 4 (**a**) Measured reflectance of the etched Si SWG structures in 5 sccm of $SiCl_4$ plasma at 25 W and 10 mTorr as a function of wavelength for the periods of 300 nm, 400 nm, and 500 nm and (**b**) influence of the period of Si SWG structures on the reflectance as a function of the wavelength for a cone height of 300 nm. The inset of (**a**) shows the SEM images of the Si SWG structures with different periods

substrate. The reflectance spectra also depend on the period of the Si SWG structures. Due to the reduced packing density, the reflectance was, on the whole, increased with the increase of period as shown in the SEM images. As the period of the SWGs was increased, the low-reflectance band shifted towards the longer-wavelength region and its minimum values were increased. The Si SWGs with the periods of 400 nm and 500 nm exhibited relatively high reflectance in the visible wavelength range. However, this is not desirable for solar cell applications. For theoretical analysis, the reflectance calculations of Si SWG structures were carried out by using the RCWA method. The model was constructed by the mean shape of the SEM image and it was assumed to be a truncated cone for simplicity. Figure 4b shows the influence of the period of Si SWG structures on the reflectance as a function of the wavelength for a cone height of 300 nm. The discrepancies between the measured and calculated results are attributed to the difficulty in matching exactly the geometric simulation model to the actual fabricated structure. However, the calculated results indicate a similar overall trend to the experimental data. The low-reflectance band broadens and shifts towards the higher-wavelength region with increase of the period of the Si SWGs. For periods above 300 nm, the band splits into two bands with reflectance of less than 0.5%, including a band which is independent of the period of 200–450 nm at wavelengths of around 600 nm. This implies that low reflectance in a specific wavelength range can be obtained by adjusting the Si SWG period without changing its height.

Figure 5a shows the measured reflectance spectra of optimized Si SWGs at different angles of incident light using a spectroscopic ellipsometer. Linearly polarized light was used, as defined with respect to the plane of incidence in the inset of Fig. 5a. The system was calibrated with a Si

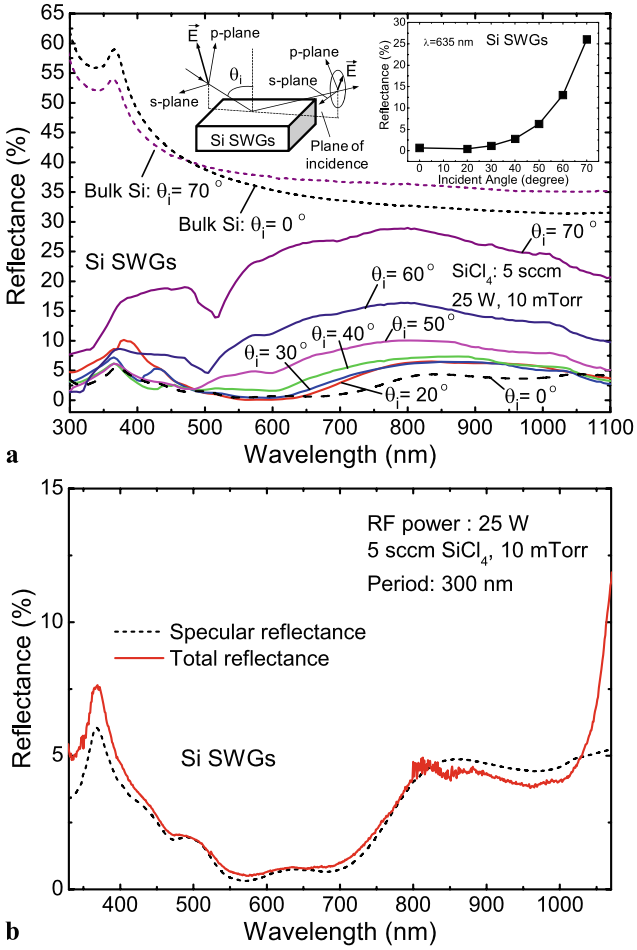

Fig. 5 (**a**) Measured reflectance spectra of the optimized Si SWGs at different angles by linearly polarized light incidence using a spectroscopic ellipsometer and (**b**) measured reflectance spectra of the optimized Si SWGs at normal incidence in specular and total reflectance modes. For comparison, the reflectance spectra of bulk Si at $\theta_i = 0°$ and $\theta_i = 70°$ are also shown in (**a**). The inset of (**a**) shows the measured reflectance as a function of incident angle of light at $\lambda = 635$ nm for the optimized Si SWGs

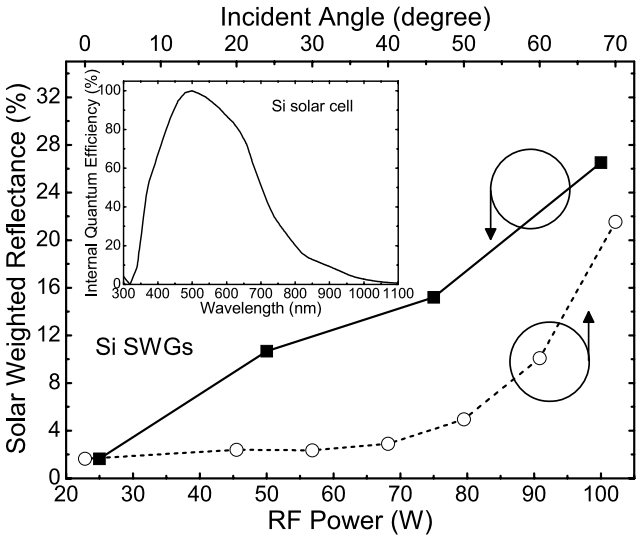

Fig. 6 Solar-weighted reflectance as functions of incident angle of light and RF power for Si SWGs

substrate and the incident angle was varied from $\theta_i = 20°$ to $\theta_i = 70°$. The dashed line show the reflectance spectrum obtained from the UV–Vis–IR spectrometer at normal incidence ($\theta_i = 0°$). The reflectance spectra of bulk Si at $\theta_i = 0°$ and $\theta_i = 70°$ are also shown in Fig. 5a for comparison. The inset shows the measured reflectance as a function of incident angle of light at $\lambda = 635$ nm for optimized Si SWGs. The reflectance was kept low for the incident angles up to $\theta_i = 40°$ over a wavelength range of 300–1100 nm. The reflectance spectrum was significantly shifted upward across the entire wavelength range above $\theta_i = 60°$, exhibiting the reflectance of more than 15%. However, the reflectance at $\theta_i = 70°$ is still lower than that of the bulk Si substrate at $\theta_i = 0°$ and $\theta_i = 70°$. For bulk Si, the reflectance at $\theta_i = 70°$ has a higher value than that at $\theta_i = 0°$ above ~475 nm while it has a rather lower value below ~475 nm. At $\lambda \sim 635$ nm, the reflectance of a Si SWG remained below ~5% up to an incident angle of $\theta_i = 50°$. The comparison between specular and total reflectances of the optimized Si SWG structure at normal incidence is shown in Fig. 5b. For total reflectance, an integrating sphere was used to capture the specularly and the diffusely reflected light from the Si SWG. The total reflectance spectrum was in good agreement with the specular reflectance spectrum over a wide wavelength range of 400–1025 nm. This means that the scattering effects in SWG structures are not considerable (i.e. almost negligible) in this wavelength range because the grating period satisfies the zero-order grating as demonstrated in other references [15, 16]. However, above $\lambda \sim 1025$ nm, the rapid increase in total reflectance is caused by the backscattered light [17].

Figure 6 shows the solar-weighted reflectance as functions of incident angle of light and RF power for Si SWGs. The simulated internal quantum efficiency (IQE) spectrum of a Si solar cell is shown in the inset of Fig. 6. The IQE spectrum was obtained with further optimization from the experimentally reported microcrystalline Si solar cell structure in [18]. The SWR, i.e. the ratio of the useable photons reflected to the total useable photons, is a useful parameter to optimize the antireflection structure of solar cells. The SWR was calculated by normalizing the reflectance spectra with the IQE spectra of a solar cell and the terrestrial air mass 1.5 global (AM1.5g) spectrum, given by [19, 20]

$$\mathrm{SWR} = \frac{\int F(\lambda)\mathrm{IQE}(\lambda)R(\lambda)\,\mathrm{d}\lambda}{\int F(\lambda)\mathrm{IQE}(\lambda)\,\mathrm{d}\lambda}, \tag{1}$$

where $F(\lambda)$ is the photon flux (i.e. AM1.5g) and $R(\lambda)$ is the surface reflectance. The overlap integral was performed in the wavelength range of 300–1100 nm, considering the absorption band of crystalline Si. As expected, the SWR was

decreased from 26% to 1.7% as the RF power was decreased from 100 W to 25 W. Clearly, the reduced reflectance of the optimized Si SWG structure is responsible for the significant improvement in SWR for Si solar cell applications. It is noted that the SWR of a multicrystalline Si solar cell with a silicon nitride antireflection layer is ∼7.8% [21]. The SWR was kept below 4.9% at $\theta_i < 50°$, indicating good antireflection characteristics over a wide range of incident angles for Si solar cells.

4 Conclusion

To reduce the surface reflection of Si for solar cell applications, Si SWG structures fabricated on Si substrates by holographic lithography and ICP etching were investigated in terms of etching parameters, together with theoretical analysis using RCWA simulation. It was found that high etch rate and etch selectivity were achieved at a low RF power of 25 W. The $SiCl_4$ plasma of 5 sccm without Ar addition exhibited a high etch selectivity of Si over PR for the fabrication of Si SWG structures. The surface reflection of Si is significantly decreased, i.e. to less than 5% over a wide wavelength range of 300–1100 nm, by optimizing the SWG structures. The reflectance depends strongly on the height, period, and shape of the Si SWG structures. Thus, the geometric Si SWG structures should be optimized for low surface reflection at the required wavelengths. The measured results of the fabricated Si SWG structures were reasonably consistent with the simulated results. From the angle-dependent measurement, the low reflectance was obtained up to $\theta_i = 50°$ for optimized Si SWGs. The low SWR of 1.7–4.9% at $\theta_i = 0$–$50°$ was achieved for Si solar cells, indicating good wide-angle broadband antireflection characteristics.

Acknowledgement The research was supported by the Basic Science and Research Program through the National Research Foundation of Korea (NRF) funded by the Ministry of Education, Science and Technology (No. 2010-0016930).

References

1. Y.F. Huang, S. Chattopadhyay, Y.J. Jen, C.Y. Peng, T.A. Liu, T.K. Hsu, C.L. Pan, H.C. Lo, C.H. Hsu, Y.H. Chang, C.S. Lee, K.H. Chen, L.C. Chen, Nat. Nanotechnol. **2**, 770 (2007)
2. S.L. Diedenhofen, G. Vecchi, R.E. Algra, A. Hartsuiker, O.L. Muskens, G. Immink, E.P.A.M. Bakkers, W.L. Vos, J.G. Rivas, Adv. Mater. **21**, 973 (2009)
3. P. Yu, C.H. Chang, C.H. Chiu, C.S. Yang, J.C. Yu, H.C. Kuo, S.H. Hsu, Y.C. Chang, Adv. Mater. **21**, 1618 (2009)
4. S.J. Wilson, M.C. Hutley, Opt. Acta **29**, 993 (1982)
5. A. Gombert, W. Glaubitt, K. Rose, J. Dreibholz, B. Bläsi, A. Heinzel, D. Sporn, W. Döll, W. Wittwer, Thin Solid Films **351**, 73 (1999)
6. M. Ishimori, Y. Kanamori, M. Sasaki, K. Hane, Jpn. J. Appl. Phys. **41**, 4346 (2002)
7. W. Wensu, S.C. Huang, A. Kechiantz, C.P. Lee, Opt. Quantum Electron. **37**, 425 (2005)
8. C.H. Sun, W.L. Min, N.C. Linn, P. Jiang, B. Jiang, Appl. Phys. Lett. **91**, 231105 (2007)
9. Z. Yu, H. Gao, W. Wu, H. Ge, S.T. Chou, J. Vac. Sci. Technol. B **21**, 2874 (2003)
10. S.A. Boden, D.M. Bagnall, Appl. Phys. Lett. **93**, 133108 (2008)
11. K. Kintaka, J. Nishii, A. Mizutani, H. Kikuta, H. Nakano, Opt. Lett. **26**, 1642 (2001)
12. Y.M. Song, S.Y. Bae, J.S. Yu, T.Y. Lee, Opt. Lett. **34**, 1702 (2009)
13. S. Chhajed, M.F. Schubert, J.K. Kim, E.F. Schubert, Appl. Phys. Lett. **93**, 251108 (2008)
14. A. Yen, E.H. Anderson, R.A. Ghanbari, M.L. Schattenburg, H.I. Smith, Appl. Opt. **31**, 4540 (1992)
15. A. Gombert, W. Glaubitt, K. Rose, J. Dreibholz, B. Bläsi, A. Heinzel, D. Sporn, W. Döll, V. Wittwer, Thin Solid Films **351**, 73 (1999)
16. M. Kuo, D.J. Poxson, Y.S. Kim, F.W. Mont, J.K. Kim, E.F. Schubert, S. Lin, Opt. Lett. **33**, 2527 (2008)
17. Y. Kanamori, K. Hane, Opt. Rev. **9**, 183 (2002)
18. S.Y. Myong, K. Sriprapha, S. Miyajima, M. Konagai, A. Yamada, Appl. Phys. Lett. **90**, 263509 (2007)
19. Renewable Resource Data Center, National Renewable Energy Laboratory. http://rredc.nrel.gov/solar/spectra. Cited 15 February 2009
20. D. Buie, M.J. McCann, K.J. Weber, C.J. Dey, Sol. Energy Mater. Sol. Cells **81**, 13 (2004)
21. Y.J. Lee, D.S. Ruby, D.W. Peters, B.B. McKenzie, J.W.P. Hsu, Nano Lett. **8**, 1501 (2008)